THE UNIVERSITY OF CHICAGO

METHODOLOGY FOR MEASUREMENT OF YOUNG'S MODULUS IN FREE-STANDING POLYMER NANOCOMPOSITE THIN FILMS

A DISSERTATION SUBMITTED TO
THE FACULTY OF THE DIVISION OF THE PHYSICAL SCIENCES
IN CANDIDACY FOR THE DEGREE OF
DOCTOR OF PHILOSOPHY

DEPARTMENT OF PHYSICS

BY
JELANI HANNAH

CHICAGO, ILLINOIS
DECEMBER 2022

I dedicate this to my ancestors who were not allowed the opportunity and who were judged for how they looked; and to anyone whose potential was ever doubted.

"And so I shall be one, with one, from one, and for one." - J. Hannah

TABLE OF CONTENTS

LIST OF FIGURES

ACKNOWLEDGMENTS

I would like to express my gratitude and appreciation to my Ph.D. advisor, Prof. Heinrich Jaeger, for his devotion, funding, and expertise, without which this work would not have been possible. During all seven years in Heinrich's lab, I gained wisdom, humility, and knowledge from him which has shaped me into being an independent scientist in Physics. I am grateful for all he has taught me for that has prepared me to contribute to the world through science.

I would like to thank my close peers and colleagues Dr. Grayson Jackson and Ted Esposito for their friendship and scientific input which has assisted me in the completion of this degree.

I would like to thank my committee members: Thomas Witten, Stephan Meyer, Sidney Nagel and David Reid for the advice and support that has enabled me to attain this doctorate degree. I would like to give another thank you to Dr. David Reid for his recruitment of me to the University of Chicago through Physics Ph.D. Bridge Program; without the bridge program this Ph.D. would not have been possible.

I would particularly like to thank Qiti Guo and Justin Jureller, Luigi Mazzenga, Yimei Chen and Phillip Griffin for training and helping me on the research facilities and helping me complete the necessary training to complete my research projects. I would like to thank former James Frank Institute researchers: Kieran Murphy, Tom Vitebaek and Leah Roth for their moral support and friendship.

I would like to thank all members of the Jaeger Lab I worked with now and the past seven years for stimulating conversations and constructive criticism: Yifan Wang, Remington Carey, Nicole James, Endao Han, Victor Lee, Melody Lim, Richa Batra, Bryan VanSaders, Tanvi Gandhi, Mike van der Naald, Hojin Kim, Baudouin Saintyves, Severine Atis, Qinghao Mao, Brady Wu, Nina Brown, Jon Kruppe, Issac Harris, Sam Livermore, Abhi Signh and Tali Khain.

Most importantly I would like to thank my parents Dr. Paul Hannah and Dr. Martha

Hernandez for their dedication to outstanding parenting that has shaped and molded me with character traits of strength, conviction, morality and self-awareness which was necessary for my development into manhood and provided the unwavering determination needed to complete this doctorate degree.

ABSTRACT

The mechanical properties of polymer nanocomposite thin films are central to their applications. Providing a non-contact and substrate-free thin film characterization method, bulge tests have many advantages to determine the mechanical behavior of free-standing thin films. In these tests the film is draped over a hole and subjected to a pressure differential which deforms, or bulges, it. In particular, bulge test allows for easy measurement of the Young's modulus, which characterizes the linear elastic response to applied strain or stress. Bulge tests furthermore are amenable to cyclic loading and time dependent creep measurements. However, previous work utilizing bulge tests used experimental approaches that either were slow in extracting film deflection data or did not directly measure the film deflection at each point in real time. In this thesis I discuss combining bulge tests with advanced, laser-scanning confocal microscopy to obtain the 3D profile of bulged films in less than 10 seconds. From the maximum height of the film deflection the Young's modulus can be extracted by approximating the bulge as a spherical cap. I apply this technique to obtain the Young's modulus of free-standing polymer nanocomposite (PNCs) thin films, which have the potential to be integrated in high-demand applications such as drug delivery, energy storage, novel packaging, and membrane filtration.

CHAPTER 1

INTRODUCTION

Accurate and robust physical property measurements are crucial for the integration of nanomaterials in devices such as batteries, photovoltaics, drug delivery for nanomedicine and water filtration.[1–8] Specifically, understanding the mechanical properties is paramount for device performance, reliability, and fabrication. One mechanical property which is of great importance when probing the deformation response of a material is the elastic modulus, or Young's modulus, E. The Young's modulus is a measure of material stiffness or resistance to deformation under an applied tensile or compressive load in the regime of linear elastic response, i.e., for small deformations. It is computed as the ratio of stress over strain, $E = \frac{\sigma}{\epsilon}$ and is expressed in units of Pascal (Pa). Here the tensile or compressive stress σ is the force per unit cross-sectional area exerted on the material and $\epsilon = \frac{\Delta l}{l}$ is the associated strain, i.e., the change in length of the material Δl, divided by the original length, l. Since the Young's modulus is an intrinsic property, every material will have a different, characteristic value of E. Materials such as metals, plastics, or ceramics have modulus values from $\sim$ 0.1-1000 Giga Pascal (GPa), with hard plastics in the 2-10 (GPa) range, metals 15-400 (GPa) and ceramics 200-600 (GPa).[7] Conventional measurements of the Young's modulus consist of tensile testing whereby a macroscopic piece of material is uniaxially stretched. For macro-scale materials this is a robust technique. However, for thin film materials that are of nanometer thickness this technique will not work. Therefore, different approaches are needed to measure the Young's modulus of thin films. These approaches need to be robust but also conducive to the films' fragility and to any sample size limitations.

Mechanical testing of nanometer-thin films can be subdivided in two categories. The first considers thin films that are bonded across their entirety to a supporting, thicker substrate (substrate-supported films). The second considers films that are free-standing, similar to a drumhead or a clamped membrane. These films are placed across an open frame and are

only supported where they meet the frame (free-standing films). Whereby approaches for supported films are often investigated by SIEBIMM (strain-induced elastic buckling instability for mechanical measurements), free-standing films have been probed by AFM (Atomic Force Microscopy) and by Nanobubble Inflation or Bulge Tests.

The basic principles of these four techniques are the following: SIEBIMM extracts the Young's modulus by measuring wrinkle formation when both substrate and film are compressed; AFM operates via the use of a cantilever that applies a point load on the film's surface and detects the deformation; Nanobubble Inflation suspends a thin film over an array of tiny holes which are then positively pressurized, producing bubbles with a measurable height profile as function of pressure. Finally, the Bulge Test is a technique closely related to the nanobubble inflation but uses a single, large hole over which the film is suspended and pressurized.

For the purposes of this thesis, I will focus on the motivation, formalism, and analysis, both qualitative and quantitative, of Bulge Test Measurements. Bulge Test Measurements have been utilized for over 70 years[1] making them an industry standard for characterizing mechanical properties of thin films. Fabrication of the fixtures for bulge tests requires considerable care to arrive at reliable results, but is, in principle, straight forward. However, accurate measurement of film deflection with varying pressure, and reliably finding the peak position of a pressurized bulge are more involved. Specifically, much depends on the instrumentation used to acquire the height profile from the bulged film. In the next four chapters I will introduce a new method for bulge tests that is based on fast-scanning confocal microscopy. This method differs from SIEBIMM, AFM and Nanobubble Inflation by the use of state-of-the-art optics that enable high-speed, high-resolution imaging of a bulged film. I then apply this method to free-standing polymer nanocomposite (PNC) thin films that consist of a Polystyrene (PS) or Polymethylmethacrylate (PMMA) polymer matrix embedded with unfunctionalized iron III oxide nanoparticles. I report on the elastic response and

structural morphology of such films fabricated under room temperature conditions (without annealing).

REFERENCES

[1] Small. M, Nix. W. D. Analysis of the accuracy of the bulge test in determining the mechanical properties of thin films. *J. Mater. Res.* 7, No.6, (1992).

[2] Huang. C. K, Lou. W. M, Tsai. C. J, Tung-Chuan. Wu, Lin. Hung-Yi, Mechanical properties of polymer thin film measure by bulge test. *Thin Solid films* 515, 7222-7266 (2007).

[3] He. J, Kanjanaboos. P, Frazer. N. L, Weis. A, Lin. X. M, & Jaeger. H. M. Fabrication and mechanical properties of large-scale freestanding nanoparticle membranes. *Small* 6, 1449-1456 (2010).

[4] Mueggenburg. K. E, Lin. X. M, Goldsmith. R. H, Jaeger. H. M. Elastic membranes of close-packed nanoparticle arrays. *Nat. Mater.* 6, 656-660 (2007).

[5] Kanjanaboos. P, Joshi-Imre. A, Lin. X. M, & Jaeger. H. M. Strain patterning and direct measurement of Poisson's ratio in nanoparticle monolayer sheets. *Nano Lett.* 11, 2567-2571 (2011).

[6] Schlicke. H, Leib. E, PetrovA, Schröder. J, and Vossmeyer. T. Elastic and Viscoelastic Properties of Cross-Linked Gold Nanoparticles Probed by AFM Bulge Tests. *J. Phys. Chem. C* 118, 4386-4395 (2014)

[7] Jancar. J, Douglas. J. F, Starr. F. W, Kumar. S. K, Cassagnau. P, Lesser. A.J, Sternstein. S. S, and Buehler. M. J. Current issues in research on structure-property relationships in polymer nanocomposites. *Polymer* 51, 3321-3343 (2010).

[8] Stafford. C, Harrison. C, Beers. K, Karim. A, Amis. E, Vanlandigham. M, Kim. H, Volksen. W, Miller. R, and Simonyi. E. A buckling-based metrology for measuring the elastic moduli of polymeric thin films. *Nature Mater.* 3, 545–550 (2004).

CHAPTER 2

METHODS FOR CHARACTERIZING MECHANICAL PROPERTIES OF THIN FILMS

Historically thin films have been characterized through a myriad of ways. Specifically, the mechanical testing and probing have predominantly relied on two methods of film preparation: 1.) free-standing films and 2.) supported films. In this chapter I will discuss past work and limitations of both approaches.

2.1 Substrate-Supported Films

SIEBIMM

A technique termed SIEBIMM (strain-induced elastic buckling instability for mechanical measurements) can be used to compute the elastic modulus of thin films that are laminated to a soft, deformable substrate. This technique was first demonstrated by Stafford *et al.*[2]

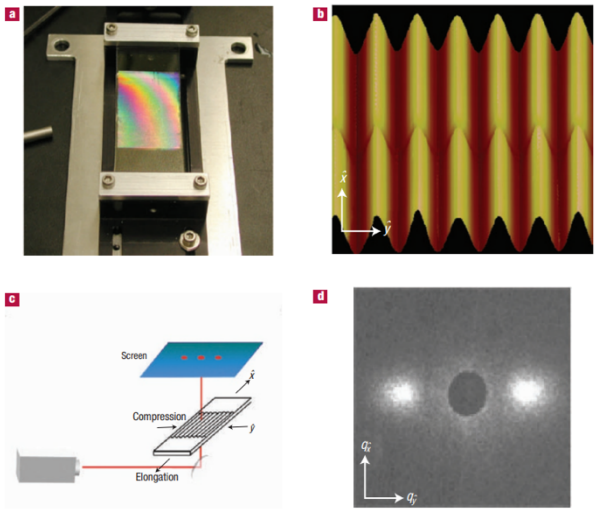

Figure 1. SIEBIMM. (a) Straining apparatus with film on PDMS substrate. (b) AFM image of buckled film. (c) Light scattering apparatus for diffraction pattern of buckled film. (d) Diffraction pattern of buckled film. Taken from C. Stafford, *Nature Mater.* 3, 545–550 (2004).

Samples for SIEBIMM are prepared by transferring a thin film from a silicon or mica substrate to the surface of a thick slab of polydimethylsiloxane (PDMS). The PDMS/film laminate is mounted onto a customized straining stage. A buckling instability is induced by an applied compressional strain, as shown in Figure 1. The buckling instability is a result of the balance between the energy required to bend the stiff upper film and the energy required to deform the soft underlying substrate.

There exists a critical wavelength that minimizes the total strain energy in the system, and this wavelength is dependent on the material properties of both the film and substrate. Assuming a sinusoidal waveform of the buckling instability, the critical wavelength d can be expressed as

$$d = 2\pi t \left[\frac{(1 - v_s^2)E_f}{3(1 - v_f^2)E_s)} \right]^{1/3} \tag{1}$$

where t is the thickness of the film, v is the Poisson's ratio, and E is the Young's modulus. Subscripts f and s relate to the film and the substrate, respectively.

SIEBIMM was used by J. Lee *et al.*[1] to measure the mechanical response of nanocomposites comprising of cadmium selenide (CdSe) nanoparticles, 3.5 nm in diameter, blended into a polystyrene (PS) matrix (Mw = 131K g/mol). To attain well-dispersed nanoparticles within the polystyrene matrix, short polystyrene ligands (Mw = 1000 g/mol) were used to functionalize the nanoparticle surfaces.[1] Film thickness ranged from 180-210 nm.

Figure 1a shows the SIEBIMM measurement apparatus used to characterize the CdSe functionalized polymer nanocomposite. Figure 2a is an illustration of the SIEBIMM technique used specifically for PS-CdSe PNC thin films. In Figure 2b a plot of elastic modulus vs nanoparticle loading (by percent weight fraction) is shown, together with the glass transition temperature T_g, where the elastic modulus was computed from SIEBIMM measurements.

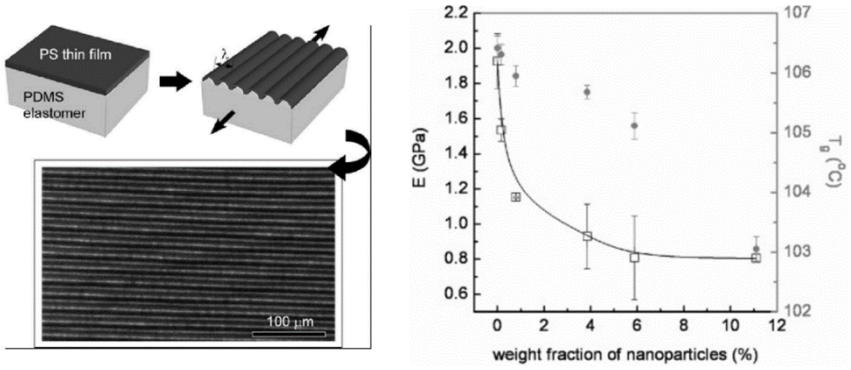

Figure 2. SIEBIMM for PNCs. (a) SIEMBIMM schematic for PS-CdSe PNC. (b) Measured PNC elastic modulus vs. nanoparticle weight percent. Taken from J. Young *et al.* *Macromolecules*, 40, 7755-7757 (2007).

2.2 Free-Standing Films

Nanobubble Inflation

A study that extracted the thermal viscoelastic properties from measuring the deformation of free-standing films is the nanobubble inflation work by McKenna *et al.*[3] The material used in this study was a PVAc poly (vinyl acetate) polymer. Films of PVAc were fabricated by spin coating 2% to 3.5% weight percent solutions of the polymer in toluene onto glass slides. After drying, the films were floated off the glass slides onto water and transferred to a filter substrate. This filter substrate consisted of a silicon nitride layer about 1 mm thick on a silicon support layer into which an array of 24 1.2-μm diameter holes was etched.

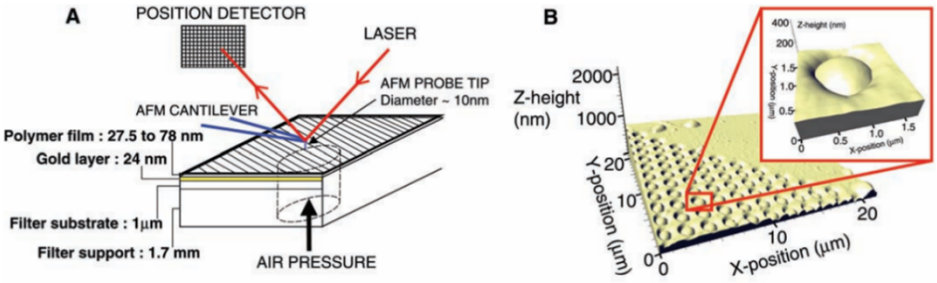

Figure 3. (a) Schematic of nanobubble inflation. (b) 3D image of individual bubble after inflation. Taken from P. A. O'Connell *et al.* *Science* 307, 1760-1762 (2005).

In this technique a pressure differential is applied uniformly across the film and the substrate, resulting in inflation of the film where it extends across a hole in the substrate and the creation of a small hemispherical bubble (Figure 3). This study was done in 2005, which at the time and still today represents a major advancement of nanomechanical testing. The technique used the imaging capability of the AFM to perform the deformation measurements, thereby removing problems associated with contact mechanics that come into play when the AFM is instead used as an indentation machine.[3]

From the bubble geometry, parameters such as the stress on the film (σ) can be related to the pressure, P; the film thickness, t_0; and the radius of curvature, R, of the bubble. R is calculated by taking the bubble profile and fitting it to the equation of a circle $R^2 = (x-a)^2 + (y-b)^2$. In this formula x and y are the x-position and y the bubble height, and the parameters a and b are constants. Extracting the radius of curvature twice, once for the unpressurized bubble (R_0) and once for the pressurized bubble (R) then gives the stress as

$$\sigma_{11} = \sigma_{22} = \frac{PR}{2t_0} \tag{2}$$

and the strain as

$$\epsilon_{11} = \epsilon_{22} = \frac{s}{2R_0} - 1 \tag{3}$$

Here, s is the segment length of the inflated bubble. The indices indicate that in an inflated bubble or hemisphere with equal radii of curvature in two orthogonal directions the associated (radial and circumferential) stresses and strains are equal. Since thermal viscoelastic response was the focus for this particular study by McKenna *et al.*, the stress and strain terms were used to calculate, as function of time and temperature, the creep response rather than the modulus. However, from Equations (2) and (3) the biaxial modulus is easily obtained as the ratio of stress and strain (see Equation (4), below).

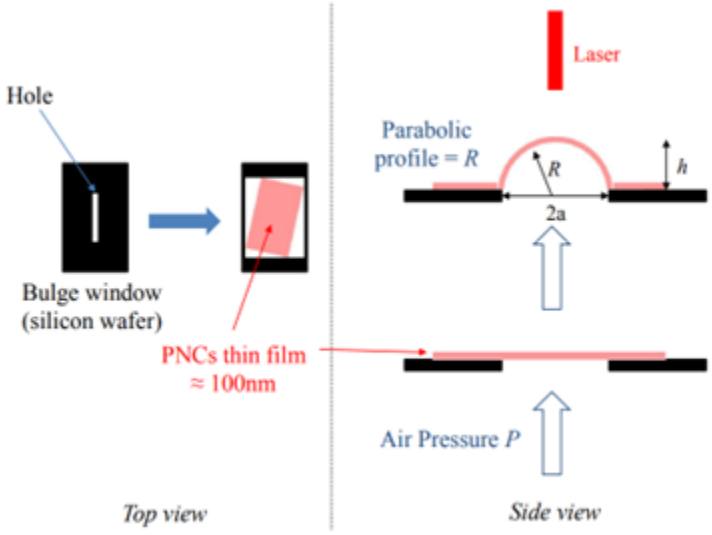

Figure 4. Bulge Test Apparatus. (a) Sample mount. (b) Illustration of confocal laser setup to measure height profile. Taken from A. Hashemi *et al.*, *NanoLett.* 15, 5465-5471 (2015)

Laser Confocal Bulge Test

In an effort to realize robust and high throughput mechanical characterization of PNC films, past work showed that free-standing films provide an alternative to substrate-supported films. One of these was a study by A. Hashemi *et al.*[4] This study discusses the advantage in grafting nanoparticles to the polymer matrix, resulting in an enhanced elastic modulus as function of weight fraction and polymer molecular weight (Mw). Specifically, hydrogen bonding silica nanoparticles grafted with tethers functionalized with 2-ureido-4-pyrimidinone (UPy) units were incorporated into a polymer matrix. Motivated to achieve excellent dispersion the study reports the H-bonding between the OH- group on the vinylphenol moieties in the matrix and the nitrogen of the ligand grafted on the NPs ensures good miscibility, and the consequences of this improved miscibility on mechanical properties were shown. The mechanical response of UPy grafted silica NPs incorporated in poly(methyl methacrylate) (PMMA) matrices in the glassy state demonstrates that both good NP dispersion and strong adhesion between the NP and the matrix are critical in increasing the elastic modulus. The

elastic modulus in this study was measured with a bulge test that used a laser confocal microscope to measure the height profile of the pressurized polymer. Shown in Figure 4 is a schematic illustration of the bulge testing apparatus. In this approach the polymer composite film was transferred onto a rectangular window in a silicon wafer. Next, the silicon wafer was mounted over an opening in a pressure chamber, with the film on the inside of the chamber. The chamber was then pressurized to deflect the free-standing portion of the film until a bulge developed. A laser scanning confocal microscope profilometer (Keyence, Inc.; with z-height resolution of 10 nm and lateral spatial resolution of 2 μm) was used to measure the film deflection and extract the radius of curvature.[5–6] The same stress strain relations shown in Equations (2) and (3) were used to compute the stress and strain. Their ratio then determines the biaxial modulus Y through

$$\sigma = Y\epsilon. \tag{4}$$

This biaxial modulus is related to the Young's modulus E, relevant for uniaxial deformation, by

$$Y = E/(1 - v), \tag{5}$$

where v is the Poisson's ratio.

The recorded data from the height profile were fitted and once R and R_0 were obtained the Young's modulus was calculated using Equations (2) - (5).

Free-standing, self-assembled gold nanoparticle membranes

Another relevant study suspended self-assembled gold nanoparticle membranes over large, micron-size holes, where the elastic modulus was computed by AFM nanoindentation measurements[7]. Nanoindentation operates by deforming a film with a local point load. From this a force vs. displacement curve is extracted. For small indentations in the center of a circular membrane

of radius R and thickness h, the force F varies with displacement δ according to

$$F = \frac{\pi E h}{3R^2}\delta^3 \tag{6}$$

This makes it possible to extract the Young's modulus E simply from the slope of a plot of force versus the cube of the displacement.

Figure 5 shows the experimental schematic of the nanoindentation measurement. It exploits the remarkable strength of Au nanoparticle membranes, where the strength of the core-ligand interaction allowed for elastic response when suspended over holes with diameters extending from 400 nm to 2 μm. Depicted also is a TEM (Transmission Electron Microscopy) image of a membrane suspended over an aperture of 250 nm radius. This demonstrates the characterization advantage of using a large, single area instead of array of holes as mentioned in the nanobubble inflation method.

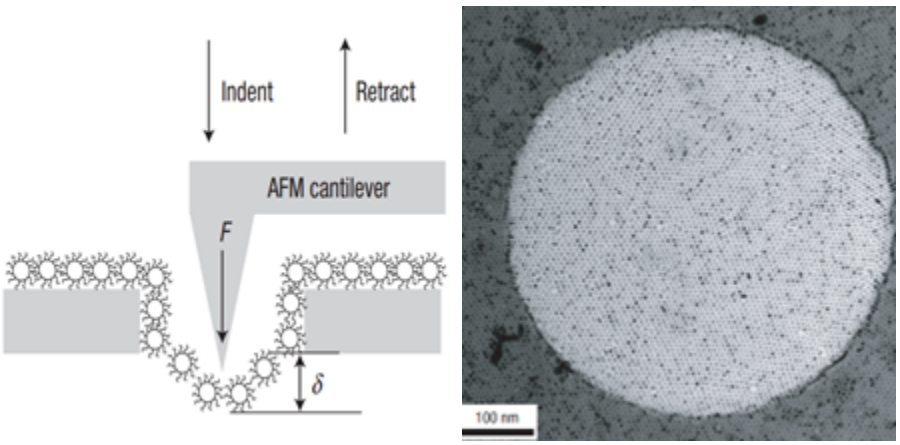

Figure 5. Nanoindentation of free-standing membrane. (a) AFM cantilever point load (b) TEM of 2D self-assembled membrane. Taken from K. E. Mueggenburg *et al.*, *Nat. Mater.* 6, 656 (2007).

AFM Bulge Test

In a study by Vossmeyer *et al.*[8] from 2014 a novel AFM Bulge Test approach was used to obtain the viscoelastic and elastic properties of cross-linked gold nanoparticles. The primary advantage of the bulge test is that membranes or films are uniformly pressurized with a load, rather than deformed by a point load as with nanoindentation.

Further, in the bulge test the mechanical properties can be sampled over large area. This provides the opportunity for fast-paced validation of material candidates for device fabrication. Shown in Figure 6a is an integrated work flow whereby an AFM sample mount was used to load and pressurize thin films. In Figure 6b is the schematic of the setup along with computer data acquisition.

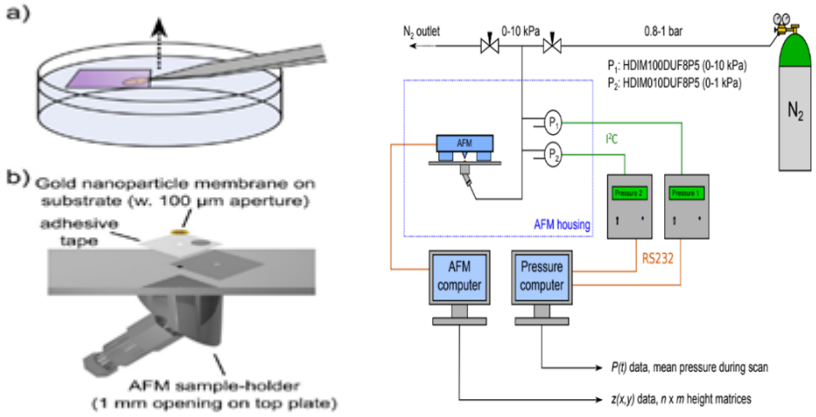

Figure 6. Illustration of AFM Bulge Test (a) Sample adhesion to pressure cavity (b) Bulge Test Overview of working pressures sensor and data acquisition. Taken from H. Schlicke, *et.al. J. Phys. Chem. C* 2014, 118, 8, 4386-4395.

Figure 7 shows a 3D rendering of the acquired height data profile after a film was pressurized. After a completed full scan, the height data were leveled based on the four areas around the dome to locate its peak. The cantilever was aligned with the peak central point of the radius of curvature in x direction and subsequent profile scans (0.977×100 μm^2, 5×512 pixel^2) were acquired traversing the central point in y direction. After peak deflections were measured, Equations (2) and (3) were used to produce a stress strain curve.

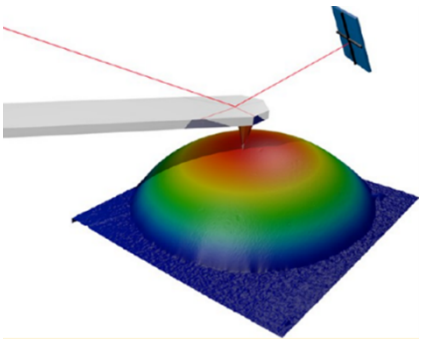

Figure 7. 3D AFM image of bulged dome height profile. Taken from H. Schlicke, *et.al. J. Phys. Chem.* C 2014, 118, 8, 4386-4395.

Using Equations (4-5) the biaxial modulus Y was the calculated. As shown by Equation (5), the biaxial modulus can be converted into the elastic modulus E with use of the material's Poisson's ratio. In this study the reported elastic modulus for free-standing film was 2.3-2.7 GPa. Another advantage of using free-standing films for bulge tests is that the thickness of the film is not required to be within ∼10 times the indentation depth, a requirement that has been noted for conventional nanoindentation studies.[8]

Comparisons of Methods: Free-Standing vs Substrate Supported

Although support substrates offer advantages in terms of the robustness and ease in film mounting, a major drawback is the time required to probe and sample the film. On the other hand, for free-standing films, the disadvantage at times is the reproducibility of film suspension. With both approaches providing their own challenges one improvement that can benefit either is the use of a state-of-the-art confocal microscope for high-throughput data acquisition. The biggest advantage of laser confocal microscopy is that it combines high optical resolution with extreme imaging speed. Together, these two aspects make it ideal for extracting height profiles of bulged films to measure mechanical intrinsic properties.

REFERENCES

[1] Lee. J, Su. K, Chan. E, Zhang. Q, Emrick.T, and Crosby. A. Impact of Surface-Modified Nanoparticles on Glass Transition Temperature and Elastic Modulus of Polymer Thin Films. *Macromolecules* 2007, 40, 7755-7757.

[2] Stafford. C, Harrison. C, Beers. K, Karim. A, Amis. E, Vanlandigham.M, Kim.H, Volksen.W, Miller. R, and Simonyi.E. A buckling-based metrology for measuring the elastic moduli of polymeric thin films. *Nature Mater* vol 3, 545–550 (2004).

[3] O'Connell P. A. and Mckenna. G. *Science* Vol 307 1760-1762 (2005).

[4] Hashemi.A, Jouault.N , Williams. G, Zhao. D, Cheng. K,Kysar. J, Guan. Z, Kumar. S. *Nano Lett.* 15, 5465-5471, (2015).

[5] Maillard. D,Kumar. S,Fragneaud. J, Kysar. J, Rungta. A, Beniecewicz. B,Deng. H, Brinson. C and Douglas. J. *J. Nano Lett.* 12, 3909, (2012).

[6] Wei.X, and Kysar. J. Residual plastic strain recovery by grain boundary diffusion in nanocrystalline thin films. *Acta. Materialia.* 59, 3937-3945 (2011).

[7] Mueggenburg, K. E.; Lin, X. M.; Goldsmith, R. H.; Jaeger, H. M. Elastic membranes of close-packed nanoparticle arrays. *Nat. Mater.* 6, 656-660 (2007).

[8] Schlicke. H, Leib. E, Petrov A, Schröder. J, and Vossmeyer T. Elastic and Viscoelastic Properties of Cross-Linked Gold Nanoparticles Probed by AFM Bulge Tests. *J. Phys. Chem.* C, 118, 4386-4395(2014).

CHAPTER 3

NEW EXPERIMENTAL METHOD FOR MEASURING YOUNG'S MODULUS VIA BULGE TESTS

In this chapter, I provide my experimental approach and description of a method based on a state-of-the-art laser confocal microscope with an in-plane resolution of 15-30nm and lateral resolution of 250 nm, which can be used together with a designed bulge testing apparatus to measure the elastic modulus of thin free-standing nanofilms. This experimental approach goes beyond prior laser-based work in that it maps out the full bulge topography and therefore can reliably and precisely identify the height of the bulge's apex for a given applied pressure. This height, together with the film geometry, is used as the key variable to extract the film's Young's modulus. A special advantage of the particular laser confocal microscope used is that all topographic measurements can be performed in a manner of 10 seconds, as compared to tens of minutes for AFM-based approaches.

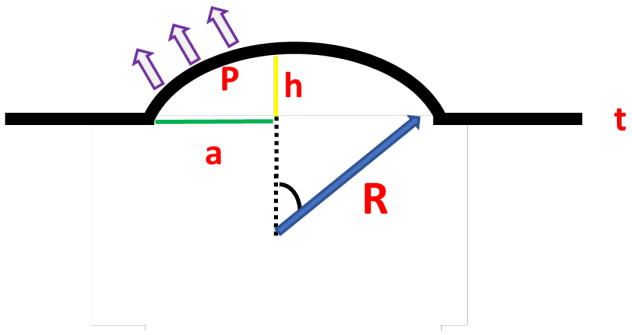

Figure 8. Spherical cap geometry.

Spherical Cap Model

Central to the analysis of any bulge test is a reliable model of the deflection of a free-standing film that has been clamped along the perimeter of a hole (here taken as circular aperture of radius a) and is subject to a pressure differential P, as shown in Figure 8. In response to this pressure differential a thin film of thickness t will experience a stress σ,

develop a bulge radius of curvature R, and, as a result, deflect up a maximum height h above its flat state for $P = 0$.

To write an expression for the modulus E one needs to express explicitly the stress and strain and then express the two as a ratio to solve for the biaxial modulus Y as a function of pressure and deflection.

The starting point is the thin-walled spherical pressure vessel formula[1] from which we can directly express the stress as $\sigma = \frac{PR}{2t}$. Now the geometrical consideration for $h << a$ is used to derive the strain term, where we can express strain geometrically as $\epsilon = \frac{R\theta - a}{a}$, where $\theta = arcsin\frac{a}{R}$ for $\frac{h}{a} << 1$. To satisfy $\frac{h}{a} << 1$ and solve for ϵ, a relation for a/R is needed. First, we can relate R, h and by using the Pythagorean theorem and expand $(R-h)^2 + a^2 = R^2$. We can simplify the expansion in terms of $R \cong \frac{1}{2h}a^2$. From the simplified relation we can write $\frac{R}{a} = \frac{1}{2}\frac{a}{h}$. Substitute $\frac{R}{a}$ back into $\epsilon = \frac{R\theta - a}{a}$ and Taylor expand $arcsin\frac{2h}{a} = (\frac{2h}{a} + \frac{1}{2}\frac{1}{3}8\frac{h^3}{a})$. The Taylor expansion simplifies the strain to the form $\epsilon = \frac{a}{2h}(\frac{2h}{a} + \frac{4}{3}\frac{h^3}{a^3}) - 1$. Altogether this gives $\epsilon = \frac{2}{3}\frac{h^2}{a^2}$ and $\sigma = \frac{Pa^2}{4ht}$, which we can solve for $Y = \frac{\sigma}{\epsilon}$. The result can be written as $P \equiv \frac{8Yt}{3a^4}h^3$.

As a final consideration for free-standing films there needs to be a formalism to incorporate a prestress σ_0. Pre-strain ϵ_0 adds to the total strain $\epsilon = \epsilon_{bulge} + \epsilon_0$, which can be written as $\epsilon = \frac{2}{3}\frac{h^2}{a^2} + \frac{\sigma_0}{Y}$. Using $Y = \frac{\sigma}{\epsilon}$ we arrive at the final form of the Spherical Cap Model for bulging a free-standing film

$$P(h) = \frac{8Yt}{3a^4}h^3 + 4\frac{\sigma_0 t}{a^2}h \tag{7}$$

Experimental Setup

Pressure-deflection curves to fit to Equation 7 were obtained by using an Olympus LEXT OLS5000 confocal microscope to probe film deflection. This microscope operates with an out of plane resolution ranging between 5-15 nm and a lateral resolution of 250 nm-500 nm.

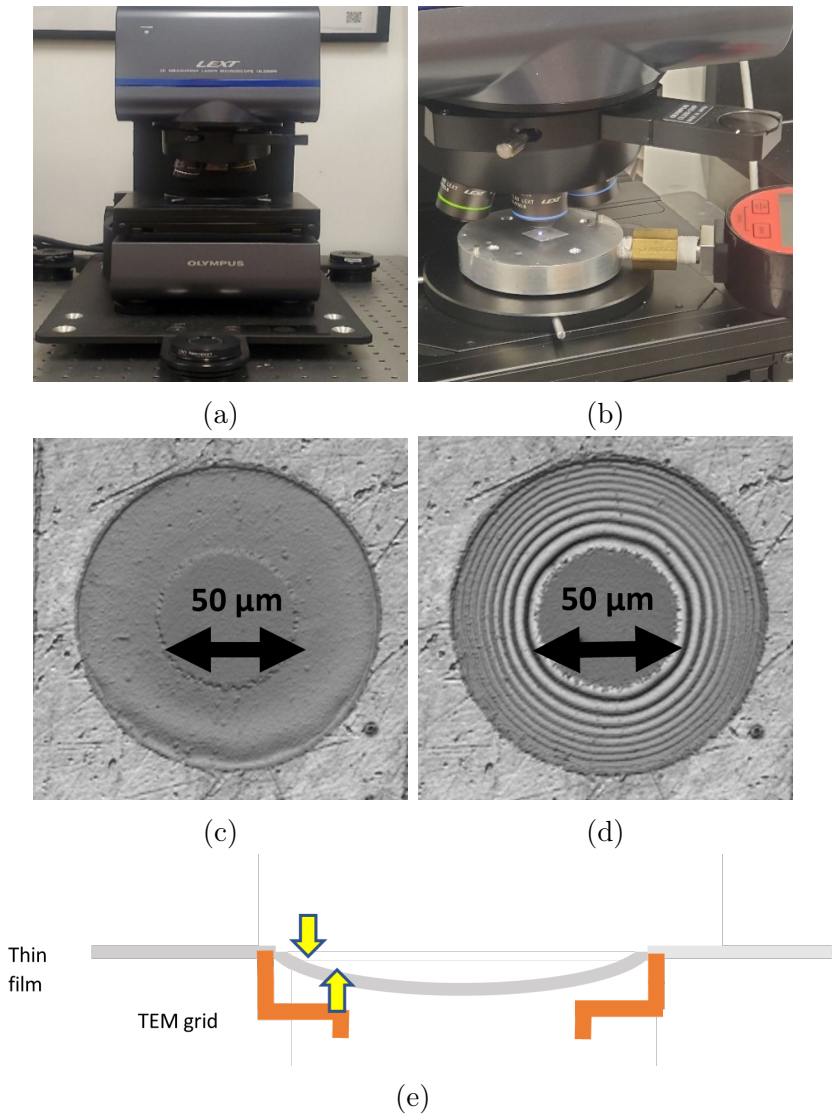

Figure 9. a,b: LEXT confocal microscope, sample holder. c,d: Free-standing film before and after pressurization at 3kPa. e: Illustration of Newton rings in the outer circle from the light interference pattern caused by the step inside the hole over which the film has been stretched d.

Films were mounted on an aluminum metal support with a central, 1 mm diameter circular hole through which vacuum was applied to bulge the films. To prevent lateral movement of the films they were mounted using double-sided adhesive tape (TESA 05338). This tape was placed over the hole on the metal support and then a hole was punched through the tape using a tapered needle that matched the diameter of the hole in the metal support.

This TESA tape was found to provide good adhesion while at the same time providing a reliable air seal, which other types of tape, such as Scotch brand tape, did not achieve.

As shown in Figure 8, the spherical cap geometry generally considers positive pressurization, whereby the bulged film points upward. For the purposes of the experiments in this thesis negative pressurization was applied to bulge free-standing films downward, as seen below in Figure 10. Films were strained uniformly by use of a vacuum pump and flexible PVC tubing that were connected to the sample holder. A large buffer chamber positioned between the vacuum pump and the sample holder was machined to act as a reservoir for static loading of the film and to dampen acoustic vibration from the vacuum pump.

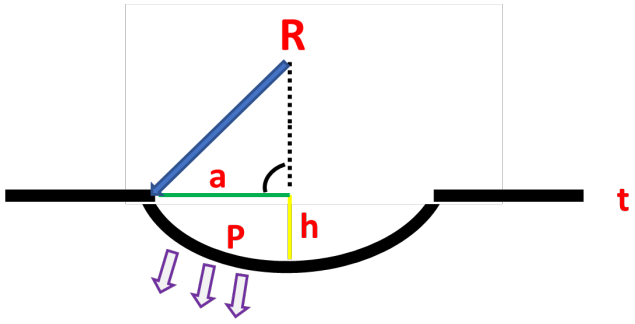

Figure 10. Spherical cap geometry of free-standing film strained by vacuum pressure.

Experimental Protocol and Data Analysis Procedure

Samples were strained by two primary methods in order resolve which method is best at preventing plastic deformation under a load-unloading cycle. The first method uses a rapid increase of deflection from zero up to the maximum, followed by a slow decrease back to zero. For this the buffer chamber is evacuated with the vacuum pump to 10 inHg, the pump is turned off, the needle valve to the sample is opened, which in a few coarse steps brings the sample to its maximum downward deflection, and then slowly air is bled into the buffer chamber to bring the chamber to ambient pressure and the sample back to zero deflection.

With the second method the deflection is slowly increased starting from zero. In this approach the buffer chamber is evacuated with the pump to 10 inHg, pump is turned off,

the needle valve is opened slightly, and this very slowly brings the sample to its maximum deflection. During this time the evolving deflection is measured every 25-30 s using the LEXT. Each scan takes less than 10 seconds. The rate of change of the deflection is adjusted, via the needle valve, to be sufficiently slow that during each LEXT scan the sample can be assumed to be in quasi-static equilibrium. The buffer chamber was pumped down to 10 inHg; however, the free-standing films are only pressurized to a maximum of 5 inHg. In order to control the applied pressure a series of course and fine needle valves were connected to the buffer chamber and sample holder. Shown in Figure 9 is a photograph of the LEXT confocal microscope and a close-up of the sample holder sitting underneath the LEXT microscope objective. Also shown are optical images, taken with the LEXT, of a film suspended over a TEM grid with a single, prefabricated hole.

In these images Newton rings around the perimeter of the hole are visible as the freely suspended film portion becomes bulged. These rings are an artifact of the particular type of TEM grid used in the experiments. The holes, or apertures, in these TEM grids through which vacuum is applied to the film have a main diameter of $\sim$50μm, but widen at the top in step-like fashion to about 75-90μm (depending on the particular batch used; the exact dimensions are measured with the LEXT in each case). This creates a circular ledge at a few microns depth underneath the suspended film. The light coming from the LEXT objective is transmitted through the transparent, downward-curved film and reflects off that ledge, which results in the Newton rings.

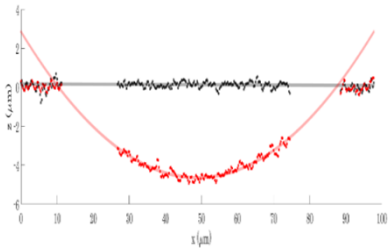

Figure 11. LEXT line traces across a freely suspended film at ambient pressure (black) and under vacuum (red). The red line is a fit to a parabola.

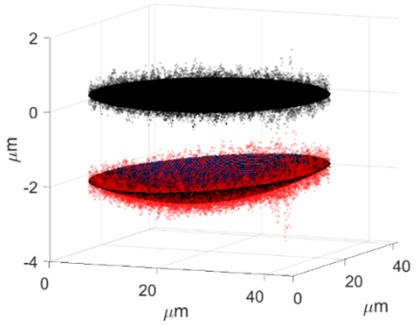

Figure 12. 3D mapping of the suspended film's surface at ambient pressure (black) and under vacuum (red). Also shown is the best-fit parabolic cap that approximates a hemispherical bulge when $h/a << 1$.

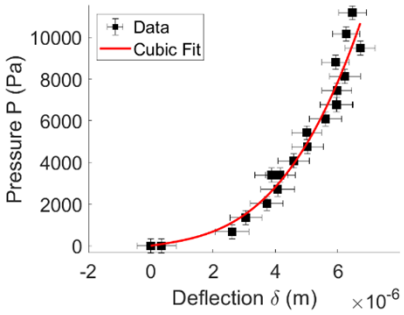

Figure 13. Pressure vs. deflection curve from loading and unloading of a free-standing film, here a 20nm thin film of a polymer. The red line is the fit to Eq. 7.

Shown in Figure 11 are LEXT line traces across the freestanding film portion prior to and after being bulged, seen in black and red, respectively. Also shown is the parabolic fit to the bulge profile, appropriately approximating a spherical cap section in the limit $h/a << 1$. The gap in the line traces arising from the same artifact from the aperture substrate that generates the Newton rings: as the LEXT laser scans across the film the detector receives backscattered light from the film surface, but also, since it transmits through the film, from the underlying ledge. Since the film is extremely thin (∼10 - 20nm) the backscattered light intensity from the ledge dominates and the LEXT's depth-measuring algorithm focuses on the ledge position deep below the film rather than on the comparatively small film deflection.

Unlike other studies mentioned above, the height h at each point across the bulge can

be obtained quickly and precisely. This makes it possible to obtain the 3D topography at given pressure, as shown in Figure 12. Typical pressure-deflection data obtained in this way is shown in Figure 13. To extract the film's biaxial modulus Y or elastic modulus E from such data a Matlab routine is used to obtain a best fit to Equation (7). The curve fit of the spherical cap model is illustrated in Figure 13. With the laser-scanning confocal microscope used in the experiments the full height profile of a bulged film can be extracted in about 10 seconds with a noise floor of 15-30 nanometers. Subsequent analysis can determine the absolute value of the maximum bulge height with an uncertainty of less than 200nm.

Figures 11-13 highlight the advancement in methodology in measuring the Young's modulus presented in this thesis. Previous studies that reported the Young's modulus of thin films [2–4] were not able to extract full topographic height profiles of a bulged film with nanometer resolution in less than 10 seconds. Particularly in the AFM Bulge Test study by Vossmeyer *et al.*[5] one full scan of the films' bulged dome took 50 minutes; in addition, subsequent line scans that transverse the peak deflection of the dome shown in Figure 7 were required just to extract a height profile and find the correct dome height h. This process is very time consuming and laborious, and it requires several steps to extract the necessary physical parameters to compute the Young's modulus.

For the spherical cap model derived in Equation (7) to be fully applicable for the purposes of analyzing the mechanical response of free-standing thin films there is a need to know how the terms in Equation (7) will represent experimental data and how well the spherical cap model can be fitted. The first term in Equation (7) is the cubic term that contains the biaxial modulus and needs to be deconvoluted from the second term which is the linear term containing the prestress. In order to explore the interplay between these two terms, a synthetic data set of pressure vs. deflections for a free-standing film was generated. In these data the physical parameters such as thickness t and radius a were fixed while the modulus and prestress were varied to elucidate how accurate the curve fit performed under various

conditions.

Shown in Figures 14-16 are three examples labelled Test 1-3, where pressure P ranges from 0-20,000 Pa, radius $a = 37$ μm, and thickness, $t = 20$ nm. The true values for modulus Y and prestress σ_0 are indicated together with the best fit values obtained from MATLAB analysis of the data using Equation (7).

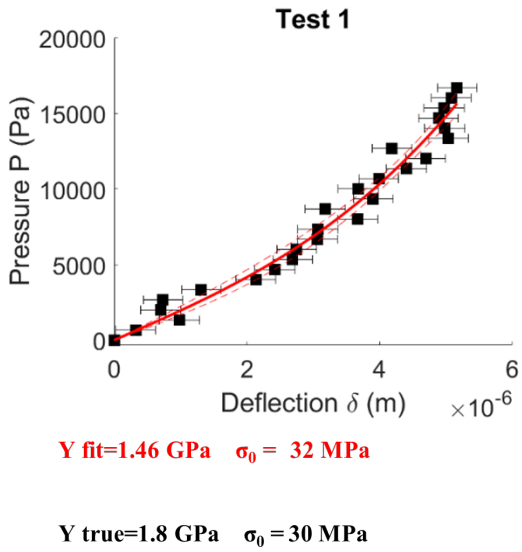

Figure 14. Test 1. The cubic and the linear term in Eq. (7) are of comparable magnitude.

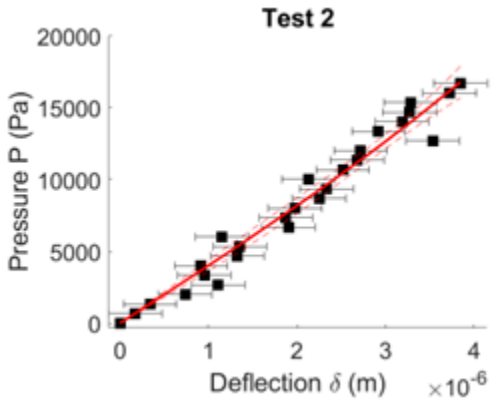

Y true=0.65 GPa σ_0 **= 70 MPa**

Y fit=0.8 GPa σ_0 **= 68 MPa**

Figure 15. Test 2. The prestress dominates.

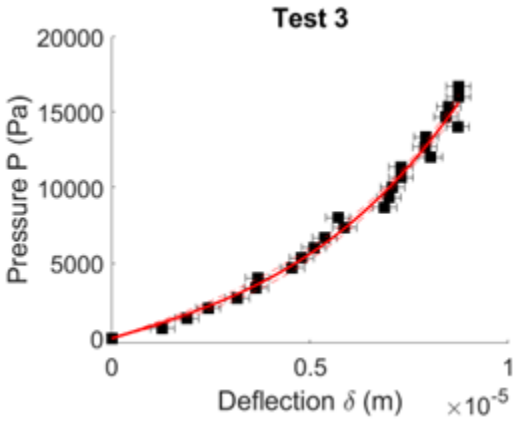

Y true=0.50 GPa σ_0 **= 12 MPa**

Y fit=0.45 GPa σ_0 **= 13 MPa**

Figure 16. Test 3. The cubic term is larger than the linear term.

The synthetic data in Figures 14-16 provides a qualitative and quantitative intuition for how different experimental results from bulge tests affect the accuracy of extracting the biaxial modulus (which then can be converted to a Young's modulus using Equation (5)). Specifically, if the prestress σ_0 dominates the cubic term, the curve will be linear and accurate determination of the modulus will not be possible.

REFERENCES

[1] Park. J, An. K, Hwang. Y, Park. J.-G, Noh. H-.J, Kim. J.-Y, Park. J.-H, Hwang. N.-M, Hyeon. T. Ultra-Large Scale Syntheses of Monodisperse Nanocrystals. *Nat. Mater.* 3, 891-895, (2004).

[2] Wei. X, and Kysar. J. Residual plastic strain recovery by grain boundary diffusion in nanocrystalline thin films. *Acta. Materialia.* 59, 3937-3945 (2011).

[3] Hashemi. A, Jouault. N, Williams. G, Zhao. D, Cheng. K,Kysar. J, Guan. Z, Kumar. S. *Nano Lett.* 15, 5465-5471, (2015).

[4] Maillard. D,Kumar. S,Fragneaud. J, Kysar. J, Rungta. A, Beniecewicz. B, Deng. H, Brinson. C and Douglas. J. *Nano Lett.* 12, 3909, (2012).

[5] Schlicke. H, Leib. E, Petrov A, Schröder. J, and Vossmeyer T. Elastic and Viscoelastic Properties of Cross-Linked Gold Nanoparticles Probed by AFM Bulge Tests. *J. Phys. Chem.* C, 118, 4386-4395 (2014).

CHAPTER 4

APPLICATION OF THE METHOD TO POLYMER NANOCOMPOSITE THIN FILMS

I start Chapter 4 by introducing the experimental findings of both the structural morphology and mechanical response of free-standing polymer nanocomposite (PNC) thin films comprised of PS and PMMA polymer matrices with Fe_3O_4 particle fillers. I then end the chapter with a discussion of the experimental results and elucidate both the mechanism for the PNC morphology and elastic behavior.

Iron (III) oxide (Fe_3O_4) nanoparticle Synthesis

Fe_3O_4 nanoparticles (NPs) were synthesized via thermal decomposition of iron (III) oleate in oleic acid and 1- octadecene under an inert $N_2(g)$ atmosphere as reported by Park *et al.*[1] This synthetic protocol led to Fe_3O_4 NPs with a diameter of 8.0 ± 0.6 nm (9% dispersity, N = 848 particles). ***Caution:*** This reaction involves very high temperatures (320 °C), and great care should be taken to: (1) maintain constant stirring to prevent uneven heating and (2) ensure the thermocouple probe is always immersed in the solution. The Fe_3O_4 NPs were twice precipitated using a equivolume mixture of hexane:ethanol and dried, and then suspended in toluene at a concentration of ∼6 mg/mL.

Preparation of Polymer Nanocomposite Solution

Polystyrene (PS) and polymethylmethacrylate (PMMA) were the two polymers used for iron nanoparticle filler dispersion and dissolution. PS and PMMA (Mw = 350,000) were both purchased from Sigma Aldrich and used as received. These were dissolved in toluene at a concentration of 1 wt%. Aliquots of the Fe_3O_4 stock solution were added to

the polymer solution to achieve a NP concentration of 0.25-10 (wt%) with respect to the dissolved polymer. The solutions were dissolved under ambient conditions for 3 days and then mechanically sonicated. Dispersion was checked by the absence of a precipitate upon centrifugation.

Free-standing Film Fabrication

Free-standing polymer thin films were prepared via spin coat deposition (using the SPS 6700 spin coater in the MRSEC Materials Preparation Lab) onto a salt crystal, which was then dissolved. A 10 mm^3 NaCl salt cube was cleaved with a razor and hammer and was mounted on the spin coating chuck. A 6 μL aliquot of the PNC solution was deposited on the substrate, which was then spun with a 3 s ramp time to 1500 rpm for 30 s. To remove the spin coated film from the salt crystal surface, the crystal was placed in glass petri dish filled with deionized water. After 5-10 minutes of dissolution the film detached from the salt crystal and floated to the top of the water. A 4 x 2 x 1 in^3 piece of acrylic was used as platform to hold 3 mm TEM copper substrates each with a prefabricated single hole aperture of diameter 50 μm (Ted Pella Inc).

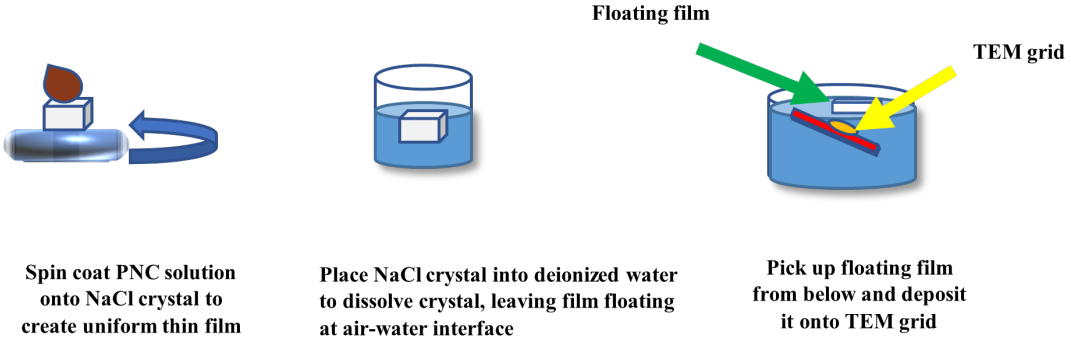

Figure 17. Free-standing film fabrication process steps (left to right)

Several TEM substates were placed on this acrylic platform and then gently submerged underwater in the petri dish and brought into contact with the floating PNC film, which

then draped over the 50 μm hole and formed a free-standing film. Fabricated free-standing films were left to dry for 30 min to 1 h before bulging for characterization. The process of fabrication is shown in the cartoon form in Figure 17.

Transmission Electron Microscopy (TEM)

Structural morphology characterization was done by using the FEI Spirit TEM. The FEI Spirit uses a LaB6 filament producing a 120 kV accelerating voltage. Films are suspended on a TEM substrate with a 300μm hole. Morphology measurements are then taken by loading individual samples in the FEI Spirit. Before inserting the sample, the beam was spread to fully occupy the phosphor screen with a measured beam current ($\sim$50 nA). The change in nanoparticle density of each corresponding weight fraction was demonstrated by increasing the magnification (1300x – 3000x) for each image.

Measurement Calibrations

The film thickness was checked for each sample by performing a confocal height scan on a second control sample that was taken from the same film, but was mounted onto a silicon substrate without hole. This involves, first, a silicon substrate of area 5mm^2 to be cleaned and sonicated with acetone, methanol and deionized water. Second, the silicon chip is submerged under water in the glass petri dish and brought into contact with the floating PNC film. It then laminates itself onto the silicon. After the film has dried on the silicon chip it can be characterized by the LEXT OLS 5000 over an area that includes both the bare silicon substrate for reference and a flat single layer portion of the film. The 100x objective is used to raster the silicon substrate/film interface with a z-height resolution of 5 nm, scanning for changes in height. The difference gives a measurement of the film thickness. For several samples this measured thickness was confirmed by complementary AFM measurements.

The aperture radius was measured with the LEXT for accuracy and analyzed by use of

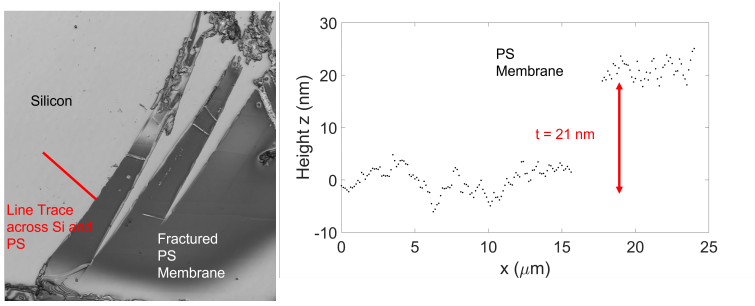

Figure 18. LEXT Thickness Measurements

MATLAB. After each film is bulged data acquired is then associated with a height profile data and optical image. The optical image shown in Figure 9 is analyzed by Matlab code where the aperture diameter is measured for each free-standing film.

Results

PNC thin films were fabricated via spin coat deposition at increasing weight fractions of Fe_3O_4 nanoparticles across the range from neat to 10 wt% for PS and neat to 6 wt% for PMMA.

a) Transmission Electron Microscopy

The transmission electron micrographs shown in Figures 19-24 for both PS-Fe_3O_4 and PMMA-Fe_3O_4 illustrate the dispersion of particles and aggregate cluster formation owing to increased density of nanoparticles with increasing nanoparticle loading. The measured size of individual iron nanoparticle diameters is $\sim$8 nm.

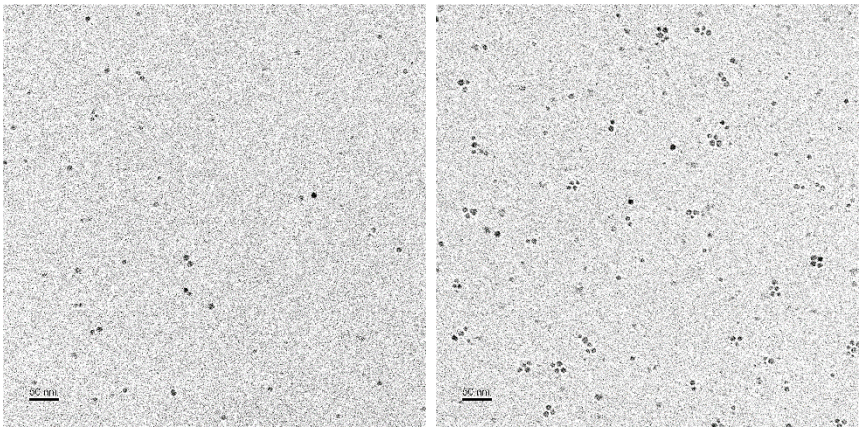

Figure 19. TEM image of PS-Fe_3O_4. Density of particles increases from 0.75 wt% (left) to 2 wt% (right).

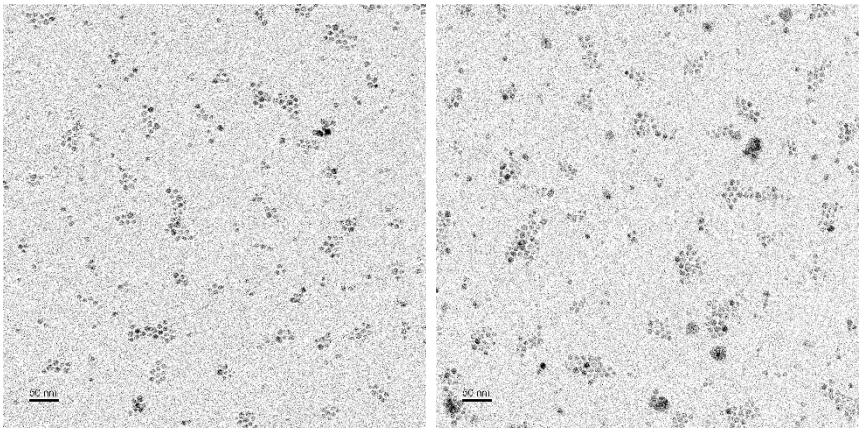

Figure 20 TEM image of PS-Fe_3O_4. Density of particles increasing with in aggregate dispersion 5 wt% (left) to 6 wt% (right).

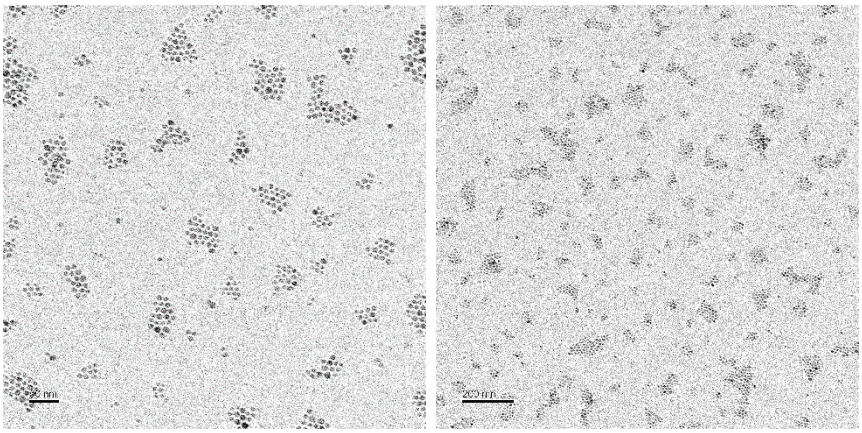

Figure 21. TEM image of PS-Fe_3O_4. Uniform aggregate dispersion at 8 wt%. The image on the left is a magnification of the image on the right.

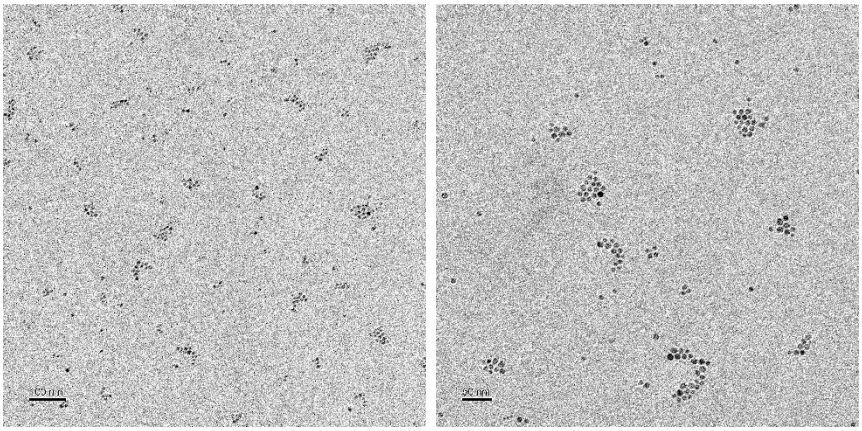

Figure 22. TEM image of PMMA-Fe_3O_4. Initial aggregate formation at 0.75 wt%. The image on the right is a magnification of the image on the left.

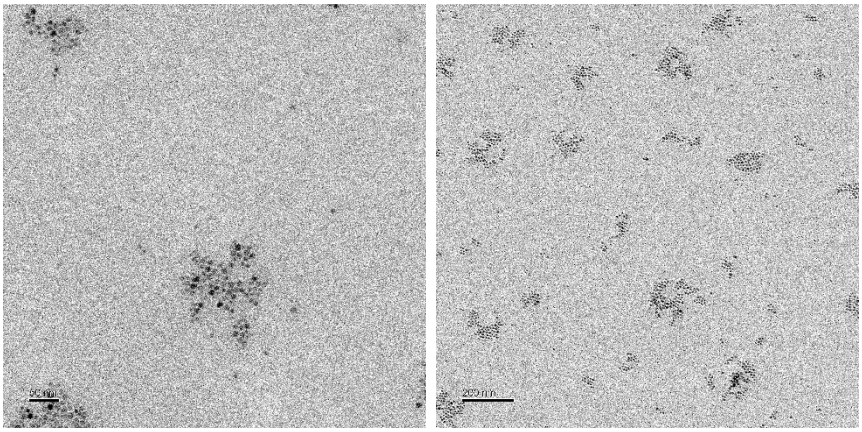

Figure 23. TEM image of PMMA-Fe_3O_4. Increased aggregate formation at 3 wt%. The image on the left is a magnification of the image on the right.

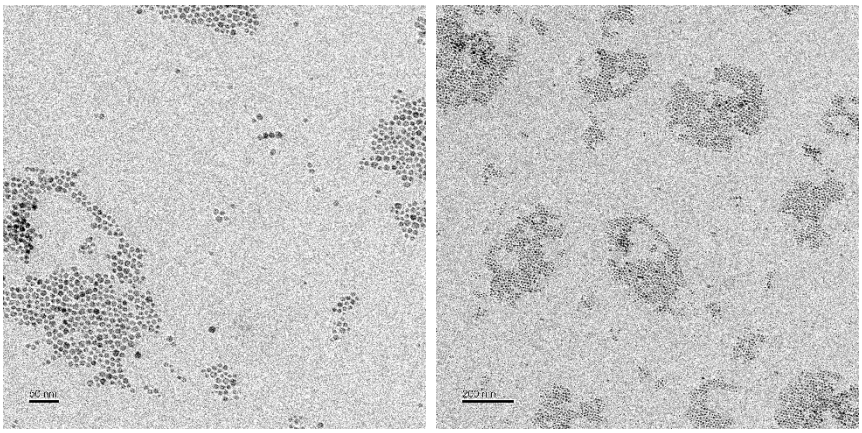

Figure 24. TEM image of PMMA-Fe_3O_4. Clustered aggregate dispersion at 5 wt%. The image on the left is a magnification of the image on the right.

b) Bulge Test Measurement Results

Figures 25-33 show pressure vs. deflection curves from the bulge tests for PS-Fe_3O_4 and PMMA-Fe_3O_4. The curves are representative for each of the film weight fractions tested. Data were obtained while the films were bulged and then unloaded back to ambient pressure. Only samples where there was negligible plastic deformation during unloading were analyzed. Each pressure vs. deflection curve has a confidence bound indicated (dotted red dashes), representing the reliability of the curve fit to the spherical cap model in Equation (7). In Figures 29 and 33, shown are outlier deflection points which correspond to experimental protocol notated in the graphs as Method 1, whereby the film was quickly pressurized to max pressure and then the pressure was released slowly. In all other pressure vs. deflection plots Method 2 was applied, whereby the film was slowly pressurized starting from zero.

The spherical cap model was used for a Matlab analysis to extract a curve fit from the pressure vs. deflection curves, and the biaxial modulus was computed. In Figures 29 and 33 the biaxial modulus Y, extracted from the curve fits, is shown as function of nanoparticle loading. The vertical error bars are from the fitting uncertainty for the biaxial modulus.

Starting with PS-Fe_3O_4 the measured biaxial modulus was found to be in the range 0.4-0.7 GPa for neat polystyrene and 0.4 GPa for 10 wt% added nanoparticles. For PMMA-Fe_3O_4 the measured biaxial modulus was 0.5 GPa for neat polymethylmethacrylate and 0.4 GPa for 6 wt% added nanoparticles. As seen from the data plots in Figures 32 and 36, there is no evidence of a systematic trend as the loading of Fe_3O_4 nanoparticles increased, implying no significant change in biaxial modulus within the uncertainties associated with the measurements. It must be noted that in Figure 29 the three data points that have the highest biaxial modulus values are possible outliers, since they were bulged by Method I as the experimental protocol, whereby the film is loaded quickly and then slowly unloaded back to zero pressure, which can more easily introduce plastic deformation than Method 2.

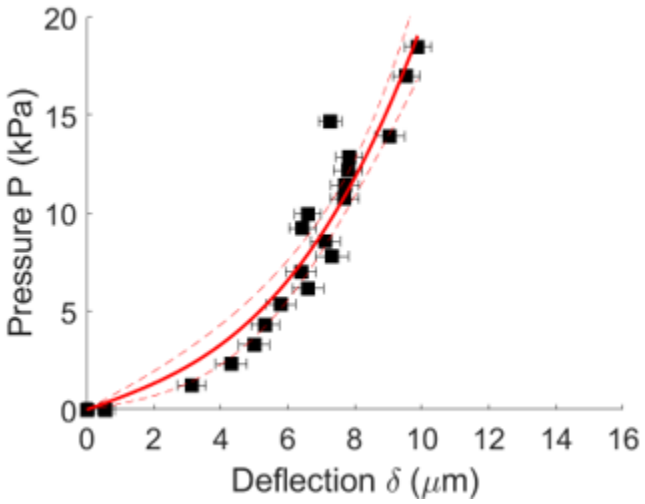

Figure 25. PS-Neat Pressure vs. Deflection Curve.

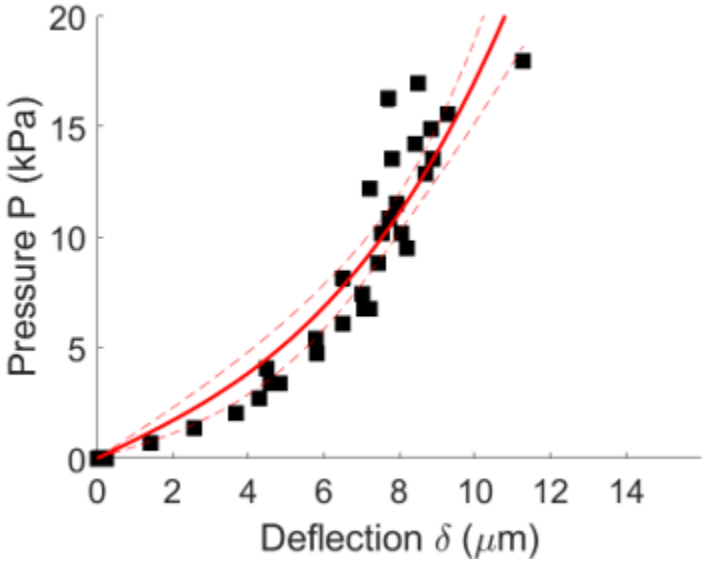

Figure 26. PS-Fe_3O_4 2 wt% Pressure vs. Deflection Curve.

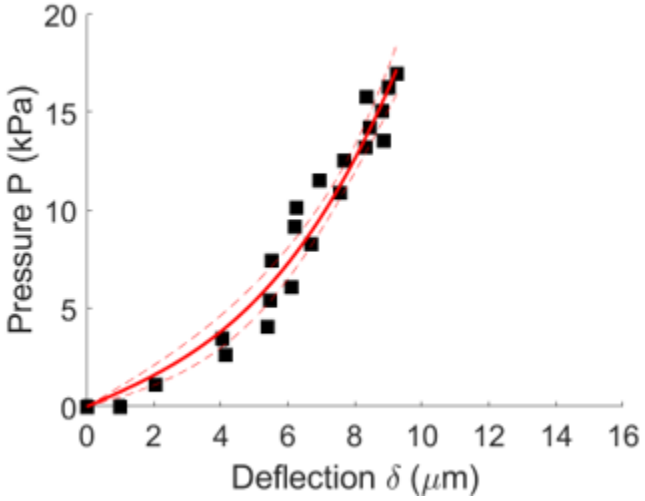

Figure 27. PS-Fe_3O_4 8 wt% Pressure vs. Deflection Curve.

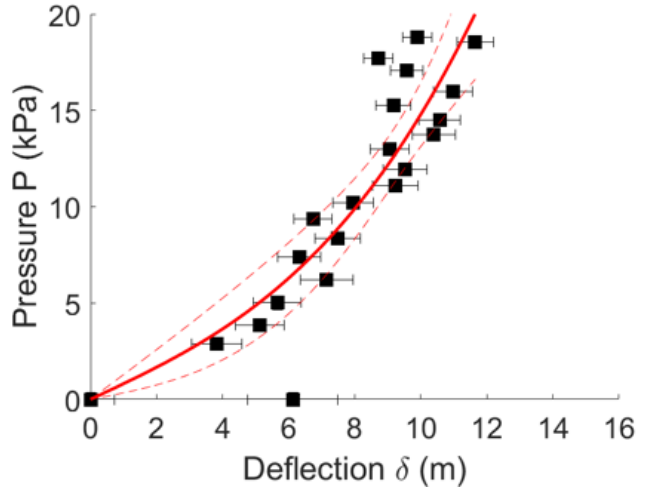

Figure 28. PS-Fe_3O_4 10 wt% Pressure vs. Deflection Curve.

PS-Fe_3O_4

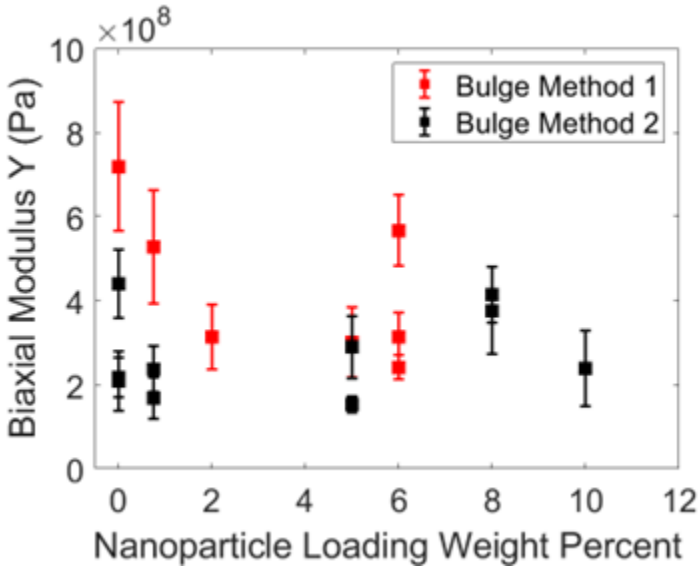

Figure 29. Biaxial Modulus vs Nanoparticle Loading Weight Percent PS-Fe_3O_4.

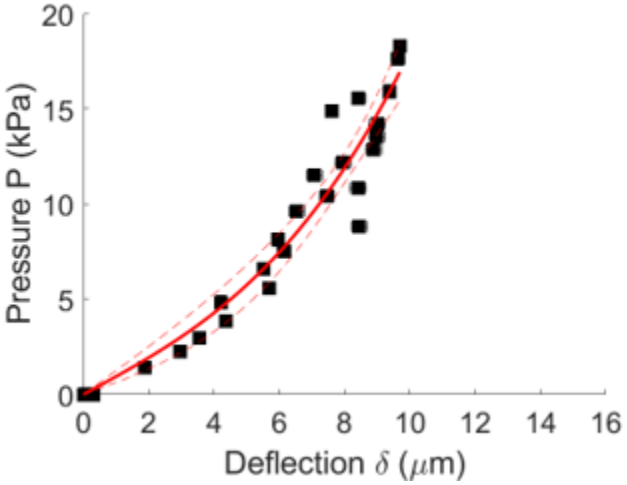

Figure 30. PMMA-Neat Pressure vs. Deflection Curve.

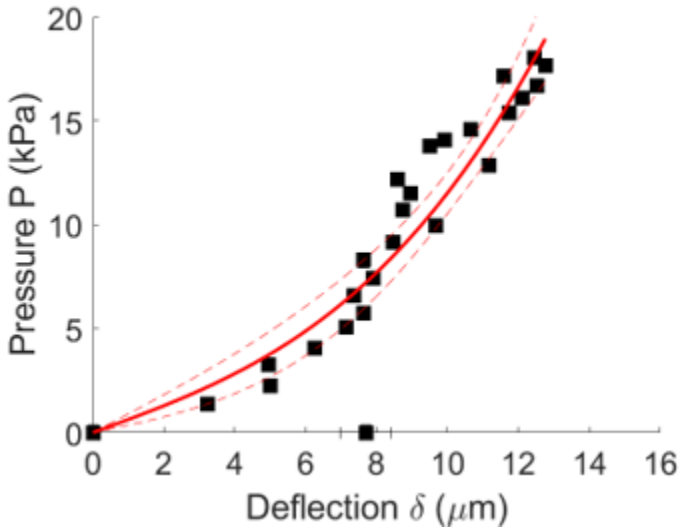

Figure 31. PMMA-Fe_3O_4 3 wt% Pressure vs. Deflection Curve.

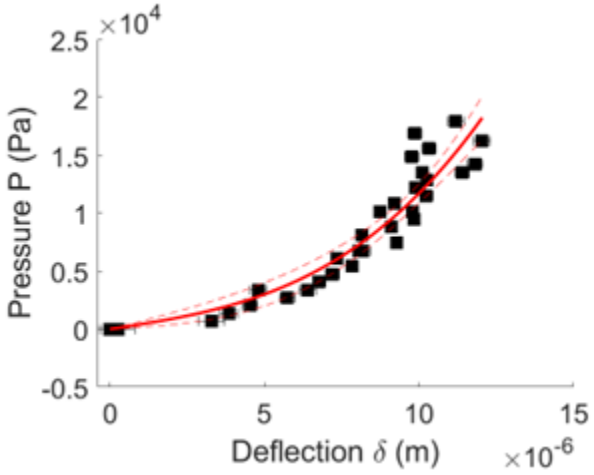

Figure 32. PMMA-Fe_3O_4 6 wt% Pressure vs. Deflection Curve.

PMMA-Fe_3O_4

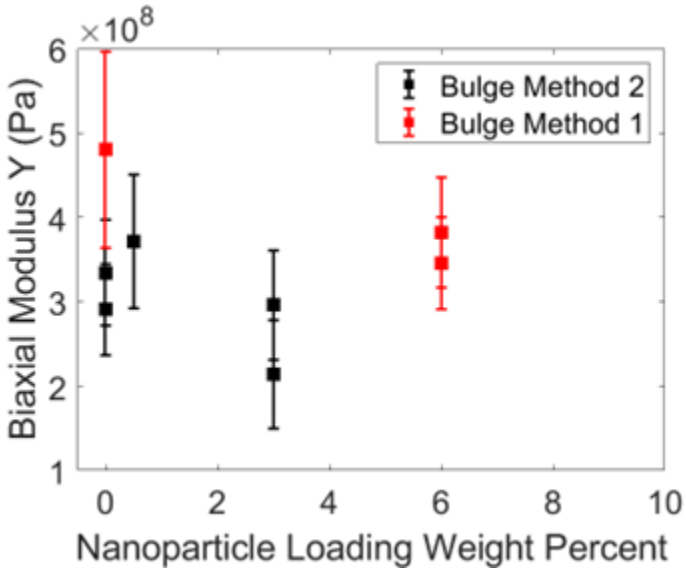

Figure 33. Biaxial Modulus vs Nanoparticle Loading Weight Percent PMMA-Fe_3O_4.

Discussion

Structural Morphology of PS-Fe_3O_4 and PMMA-Fe_3O_4

The TEM micrographs illustrate an evolution in nanoparticle density and aggregate formation. Starting with PS-Fe_3O_4 in Figures 18-20 we observe minimal particles present in the PS film at 0.75 wt%. As more particles are introduced into the PS matrix the density of particles increases, as seen when comparing 0.75 wt% and 2 wt%. This trend continues in the micrographs of PS with 5 wt% and 6 wt% Fe_3O_4; however when approaching higher weight fractions the onset of aggregate cluster formation begins and leads to a dispersion of aggregate clusters, as seen for PS with 8 wt% Fe_3O_4. The formation of aggregate clusters can originate from the weak nanoparticle-polymer interactions.[1–3] Since the nanoparticles were not functionalized in this study, the particle to polymer chain affinity is weak, resulting in nanoparticles that can detach rather easily. Further, the chemical bonds of the oleyamine ligands surrounding the Fe_3O_4 core of the nanoparticles are secondary van der Waals bonds; so ligands can also detach with relative ease, which then can lead to particle aggregation and cluster formation. Finally, the oleyamine ligands are miscible in polystyrene, meaning they are hydrophobic. This explains the ability for clusters to have good dispersion with increasing loading weight fraction.

Contrary to the morphology observed with PS-Fe_3O_4 the onset of aggregate cluster formation begins to occur at lower nanoparticle loading weight fractions for PMMA-Fe_3O_4. This early aggregate presence is likely due to PMMA-Fe_3O_4 being less miscible in solution. Fe_3O_4 nanoparticles are more hydrophilic with PMMA, resulting in non-uniform aggregate dispersion compared to the polystyrene matrix shown in Figures 24-26.

Elastic Response

The elastic response measurements for both types of polymer matrices shows that the

addition of Fe_3O_4 nanoparticles results in no systematic change, within the measurement uncertainties, in biaxial modulus as the nanoparticle loading weight percent is increased (Figures 29 and 33). This is in contrast to the increase in elastic modulus observed by Kumar *et al.*[7−8], who used chemically grafted silica nanoparticles in a PMMA matrix. We note that these particles were functionalized to hydrogen bond to the PMMA matrix. Other researchers[8−10] also reported that functionalized nanoparticles embedded in a polymer matrix result in polymer chain confinement, which leads to reduced chain mobility. Reduced mobility, in turn, was shown to increase the elastic modulus as more functionalized particles are introduced into the polymer matrix.

However, contrary to the observations of an increase in elastic modulus, there have also been reports of softening from the addition of functionalized nanoparticles, which then leads to a decrease in elastic modulus. One example is the work by Young *et al.*, shown in Figure (2). Crosby *et al.*[11] found a decrease in elastic modulus when they added Cadmium selenide nanoparticles functionalized with polystyrene ligands to a PS matrix. The reduction in elastic modulus was explained as being related to the fact that the addition of PS ligands plasticized the matrix.

We attribute the finding that the elastic modulus remains effectively unchanged with nanoparticle loading to the use of unfunctionalized nanoparticles. Such unfunctionalized particles should not interact significantly with the polymer chains and affect their mobility. Thus, we do not expect these particles to produce positive or negative trends in elastic behavior as function of nanoparticle weight fraction. This is supported by Crosby *et al.*[6] who found for similarly thin (19 nm) PMMA films that the modulus did not change with the addition of silica nanoparticles up to the maximum volume fraction of 10%.

Finally, studies in the past reported Young's modulus values for both PS and PMMA neat thin films in the range 1.5 - 2 GPa.[6,11] The values we obtained (see Figures (32) and (36)) are significantly lower. For PS-Fe_3O_4 converting the biaxial modulus Y to the elastic

modulus E using Equation (5) we find E values of 0.4 GPa, 0.2 GPa and 0.3 GPa for neat, 2 wt% and 8 wt%, respectively. For PMMA-Fe_3O_4 the E values are 0.3 GPa, 0.1 GPa and 0.3 GPa for neat, 3 wt% and 6 wt%, respectively.

We speculate that there could be several reasons for the low values. One reason might be thickness dependence. In a study by Keten *et al.*[4] simulations were conducted to investigate the thickness-dependent mechanical behavior of glassy polymer thin films. It was observed that, in thin supported as well as free-standing films, the effects of the free surfaces on the molecular structure and dynamics of polymer chains fundamentally change the behavior compared to the bulk, and that these effects become more dominant as film thickness decreases below 100 nm.[5] However, Crosby *et al.*[6,11] in two studies (one for PS and one for PMMA) investigated the stress-strain response of ultrathin free-standing polymer films and reported no change in elastic modulus for thicknesses as low as 32 nm (neat PS) and 19 nm (PMMA with silica nanoparticles). A second reason might be that the low Young's modulus for our films is due to the fabrication and film deposition process. A recent study[12] showed that absorption of water molecules can have an effect on the modulus. This could introduce a plasticizing effect from residual water when the film is transferred onto the TEM aperture hole. A third reason could be related to the fact that the oleyamine ligands that cover the Fe_3O_4 nanoparticle cores are only weakly bound to the nanoparticles cores. If some of these ligands detach, they could migrate to the film surface. An excess of ligands at the film surface has been noted to weaken and soften the mechanical properties of free-standing polymer films.[10]

In summary, the data in this thesis indicates that the addition of 8 nm diameter, unfunctionalized Fe_3O_4 nanoparticles to PS and PMMA thin films does not produce a change in biaxial or Young's modulus up after increasing the nanoparticle loading weight percent up 10 wt% and 6 wt% for PS-Fe_3O_4 and PMMA-Fe_3O_4 respectively. We attribute this to the fact that the unfunctionalized nanoparticles do not significantly interact with

the polymer chains, in contrast to functionalized nanoparticles. We speculate that the observed low value of the Young's modulus compared to literature values most likely is either the result of residual water in the films or due to excess ligands at the films' surfaces.

REFERENCES

[1] Ash. B. J., Rogers. D. F., Wiegand. C. J., Schadler L. S., Siegel. R. W., Benicewicz. B. C., and Apple. T. *Polym Compos*, 23, 1014. (2002).

[2] Jancar. J, Douglas J. F., Starr F. W., Kumar S. K., Cassagnau. P, Lesser. A. J., Sternstein. S. S. and Buehler. M. J. Current issues in research on structure-property relationships in polymer nanocomposites. *Polymer* 51 ,3321-3343 (2010).

[3] Joucalt. N, Zhao. D and Kumar. S. Role of Casting Solvent on Nanoparticle Dispersion in Polymer Nanocomposites. *Macromolecules.* 47, 5246-5255 (2014).

[4] Xia. W and Keten. S. Size-dependent mechanical behavior of free-standing glassy polymer thin films. *Journal of Materials Research*, Vol 30, 1, 36-40 0114 (2015).

[5] Huang. C, Lou. W, Tsai. C, Wu. Chuan. T and Lin. H. Mechainical Properties of polymer thin film measured by the bulge test. *Thin Solid Film.* 515, 7222-7226 (2007).

[6] Bay. R, Zarybnicka. K, Jancar. J and Crosby. A. Mechanical Properties of Ultrathin Polymer Nanocomposites. ACS *Appl. Polym. Mater.* 2, 2220-2227 (2020).

[7] Hashemi. A, Jouault. N, Williams. G, Zhao. D, Cheng. K, Kysar. J, Guan. Z, Kumar. S. Enhanced Glassy State Mechanical Properties of Polymer Nanocomposites via Supramolecular Interactions. *Nano Lett.* 15, 5465-5471 (2015).

[8] Maillard. D,Kumar. S,Fragneaud. J, Kysar. J, Rungta. A, Beniecewicz.B,Deng.H, Brinson.C and Douglas.J. Mechanical Properties of Thin Glassy Polymer Films Filled with Spherical Polymer-Grafted Nanoparticles. *Nano Lett.* 12, 3909, (2012).

[9] Kumar. S and Joucalt. N. Nanocomposites with Polymer Grafted Nanoparticles. *Macromolecules.* 46, 3199-3214 (2013).

[10] Lee. J, Su. K, Chan. E, Zhang. Q, Emrick.T, and Crosby. A. Impact of Surface-Modified Nanoparticles on Glass Transition Temperature and Elastic Modulus of Polymer Thin Films. *Macromolecules* 40, 7755-7757 (2007).

[11] Bay. R and Crosby. A. Uniaxial Extension of Ultathin Free-standing Polymer Films. ACS *Macro Lett.* 8, 1080-1085 (2019).

[12] Dolmat. M, Kozlovskaya. V, Cropek. D and Kharlampieva. E. Free-standing Thin Hydrogels: Effects of composition and pH-dependent Hydration on Mechanical Properties. ACS *Appl Polym. Mater.* 3, 3960-3971 (2021).

CHAPTER 5

SUMMARY AND FUTURE WORK

This thesis work focused on a new methodology for measurements of the Young's modulus using mechanical bulge testing of free-standing thin films. The method uses advanced laser-scanning confocal microscopy, and its main advantage is the combination of speed and ease with which measurements can be performed. I first introduced the motivation behind the method and the requirements for the computation of the biaxial modulus Y and its relation to the Young's modulus E. I provided a derivation about the geometrical parameters needed to be considered when quantitatively describing the elastic response behavior of a free-standing thin film that is being bulged by applying a pressure differential across it. With the laser-scanning confocal microscope used in the experiments the full height profile of a bulged film can be extracted in about 10 seconds with a noise floor of 15-30 nanometers. Subsequent analysis can determine the absolute value of the maximum bulge height with an uncertainty of less than 200 nm.

Second, I illustrated the new method with bulge tests of free-standing polymer nanocomposite thin films. Specifically, I studied how increasing the loading weight fraction of non-functionalized iron III oxide nanoparticles in a polystyrene and a polymethylmethacrylate polymer matrix affects the bulging behavior. Over the weight fraction ranges investigated the bulge test measurements indicated no clearly identifiable trend and, within the experimental uncertainties, suggest that there is no change in biaxial modulus resulting from the addition of unfunctionalized nanoparticles. The absolute values for the elastic modulus obtained from these experiments, in particular also for the neat films that contained no nanoparticles, were about a factor of 5 lower than expected from prior literature. This suggests that in these thin films the mechanical properties were dominated by an as yet unidentified mechanism. I speculate that this could be related to a plasticizing effect from the film fabrication procedure as well as from excess oleyamine

ligands in the films. After completion of the thesis, it was discovered that the software program called gwyddion, which is used to output height data from the proprietary Olympus file format (.poir) for subsequent batch processing using Matlab, does not preserve the correct z-scale for the height data. Corrected deflection values may be smaller by a factor of roughly two than those reported in this thesis, and therefore the correct values of the inferred modulus may be larger than those reported by a factor of roughly eight. All deflection uncertainties will also need to be reduced by the same factor of roughly two. Future work of this investigation could explore a variety of thermal analyses of this PNC system along with studying the morphology and elastic response of functionalized iron III oxide nanoparticles under external stimuli.